Materials Science and Engineering A 397 (2005) 178–189

www.elsevier.com/locate/msea

Dry sliding wear behaviors of Al–25Si–2.5Cu–1Mg alloys prepared by powder thixocasting

C.M. Chen [a,b,*], C.C. Yang [b], C.G. Chao [a]

[a] *Institute of Materials Science and Engineering, National Chiao Tung University, Hsinchu 310, Taiwan, ROC*
[b] *Industrial Technology Research Institute, MRL, J100, Rm 707, Bldg. 52, 195-5 Chung Hsing Rd., Section 4, Chutung, Hsinchu 310, Taiwan, ROC*

Received 20 October 2004; received in revised form 2 February 2005; accepted 2 February 2005

Abstract

The wear performance of an Al–25Si–2.5Cu–1Mg alloy prepared by powder thixocasting was studied using a pin-on-disc machine. LM13 and an Al–25Si–2.5Cu–1Mg alloy prepared by conventional ingot metallurgy were also investigated for comparison. The sliding tests were performed under ambient conditions and without lubricant. During the tests, the applied load was increased stepwise until wear seizure occurred. Experimental data reveal that the powder thixocast alloys exhibit better wear performance than that of conventional alloys, especially under heavy load conditions and following T6 treatment. This work demonstrates the potential of the new method, powder thixocasting, for fabricating hypereutectic Al–Si–X alloys with a high wear resistance. Moreover, the variation in the wear rate with the applied load for the alloy can be divided into three regions. The mechanisms associated with these wear regions were discussed based on the investigations of the worn subsurface and the wear debris.

Keywords: Aluminum–silicon; Sliding wear; Thixocasting; Powder processing

1. Introduction

High wear resistance, low thermal expansion, and reduced density make hypereutectic Al–Si–X alloys very attractive for transportation applications. Their most common applications are in components, such as cylinder liners, pistons, engine blocks and compressor scrolls [1]. Traditionally, these components are fabricated by casting or PM routes. However, the castings always exhibit low ductility and poor machinability because they have large primary Si particles [2]. Although traditional PM processes such as powder forging [3] or extrusion [4] offer some advantages in fabricating high-performance Al–Si alloys, they still suffer from the shortcoming of the difficulty of net shape forming the component.

Recently, the authors introduced a new method called powder thixocasting [5,6], in which the powder process and thixocasting were combined to achieve easily the net-shape forming of hypereutectic Al–Si–X components with fine and uniform primary Si particles. Thixocasting is a semi-solid forming process that forms metal components by injecting non-dentritic semisolid materials into the mold using a die-casting machine [7]. In this work, hot-densified Al–25Si–2.5Cu–1Mg prealloyed powder preforms were heated into semisolid state, before being thixocast.

The wear behaviors of the Al–Si alloys are known to depend strongly on the Si contents [8–10], processing routes [11–14] and the size and distribution of primary Si particles [15]. Besides, the wearing test conditions such as applied load, counter sliding body, and sliding speed also greatly affect the wear behaviors of the alloys [16–18]. This study seeks to elucidate the wear performance of an Al–25Si–2.5Cu–1Mg alloy fabricated by this new method. A popular commercialised piston alloy, LM13, fabricated by liquidus casting routes, and an Al–25Si–2.5Cu–1Mg alloy fabricated by conventional thixo-

* Corresponding author. Tel.: +886 3 5916987; fax: +886 3 5820207.
E-mail address: mu@itri.org.tw (C.M. Chen).

0921-5093/$ – see front matter © 2005 Elsevier B.V. All rights reserved.
doi:10.1016/j.msea.2005.02.010

Table 1
Chemical compositions of the alloys

Alloy	Processing route	Chemical composition (wt%)							
		Si	Cu	Mg	Mn	Fe	Ni	Ti	Al
Al–25SiCuMg (PT)	Powder thixocast	24.6	2.56	1.04	0.47	0.16	0.01	0.03	Bal
Al–25SiCuMg (IT)	Conventional ingot thixocast	24.2	2.25	1.08	0.08	0.69	0.04	0.08	Bal
LM13	Gravity cast	11.6	1.08	1.12	0.01	0.50	1.00	0.03	Bal

casting were examined for comparison to assess the wear performance of the powder thixocast alloys. The sliding wear mechanisms were discussed based on observations of the worn surface and wear debris obtained in this investigation.

2. Experimental

The chemical compositions of the alloys are shown in Table 1. Al–25SiCuMg (PT) alloy was produced using powder thixocasting, Al–25SiCuMg (IT) alloy was produced using conventional ingot thixocasting, and finally LM13 alloy was cast in a permanent metallic mould. Fig. 1 schematically depicts the powder thixocasting processes. At first the Al–Si–Cu–Mg prealloyed powders were hot consolidated into powder preforms, which were then heated to a semisolid temperature by induction coils. Afterward, they were immediately transferred to a sleeve and extruded into a mould cavity by a plunger of a die-casting machine. The detail procedures were published elsewhere [5,6]. In powder thixocasting of Al–25SiCuMg (PT) alloy, the feedstock was prepared by aforementioned powder process. On the other hand, the feedstock for thixocasting Al–25SiCuMg (IT) alloy was prepared by squeeze casting of the alloy at 800 °C and under 85 MPa and without any refiner for primary Si. The abbreviation IT refers to this conventional "ingot" thixocasting, which is distinct from the PT that refers to "powder" thixocasting [6].

Sliding wear tests were conducted at room temperature. The T6 condition for the Al–25Si–2.5Cu–1Mg alloys was 500 °C for four hours, followed by 175 °C for ten hours, and for LM13 alloys was 520 °C for four hours, followed by 175 °C for eight hours. Wear tests were performed using a conventional pin-on-disc testing machine. The pins, 8 mm in diameter and 15 mm long, were machined from the thixocast or cast Al–Si alloys. The disc-shaped counter material was BS 708 M40 steel whose hardness was adjusted by heat-treatment to Rockwell C 40. All tests were performed without lubricant and at room temperature. Before the wearing test, the surfaces of the aluminum alloy pins and the counterface disc were polished to a surface roughness, R_a, of under 0.1 μm. During the wearing test, the applied load was increased stepwise until the onset of specimen seizure was noted. The specimen seizure was specified by a sudden increase in coefficient of friction, which was caused by strong adhesion of the specimen material to the disc and was typically accompanied with abnormal noise in the pin-disc assembly. At each step in the wearing test, the pin was slid at a constant speed of 1.57 m s^{-1} over a distance of 1880 m under constant load. At the end of each step, the rotation of the steel disc was stopped automatically and a surface thermal couple was immediately employed to measure the bulk temperature of the pin by touching the worn surface of the pin. Then, the worn pin was withdrawn from the fixture of the wear machine and was weighed to determine the wear rate. After an interval of about 5 min, the same pin that had been worn and weighed was used again in the next step for the wearing test. The wear rate values were determined from the measured weight loss and expressed in terms of volume loss per unit sliding distance (m^3/m). Each wear rate value was averaged from the data obtained on at least two wearing pins.

The worn surfaces and debris after sliding at different loads were investigated by XRD, SEM and EDS. Subsurface microstructures were also investigated at the cross-sections perpendicular to the worn surface. Microstructures were observed using optical microscope and samples were etched using 0.5% HF water solution.

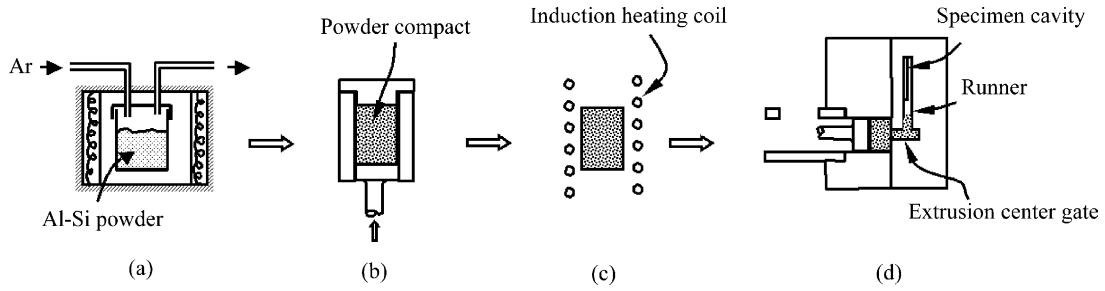

Fig. 1. Schematic diagram of the powder thixocasting procedures: (a) preheating the powders; (b) producing powder compacts; and (c) heating the compacts into a semi-solid state; and (d) net shape forming using a die-casting machine.

3. Results

3.1. Microstructure and microhardness

Figs. 2 and 3 present the optical microstructures of the as-prepared and T6-treated Al–Si–Cu–Mg alloys, respectively. These alloys were fabricated using different processing routes, so they have distinct sizes and distributions of Si particles. Notably, the powder thixocast Al–25SiCuMg (PT) alloy exhibits much finer primary Si particles than does the conventional thixocast Al–25SiCuMg (IT) alloy (approximately 8 μm against 100 μm). Besides, the Al–25SiCuMg (PT) alloy exhibits no sign of eutectic Si particles (Fig. 2a), although the Si content of this alloy exceeds the eutectic point (~12%);

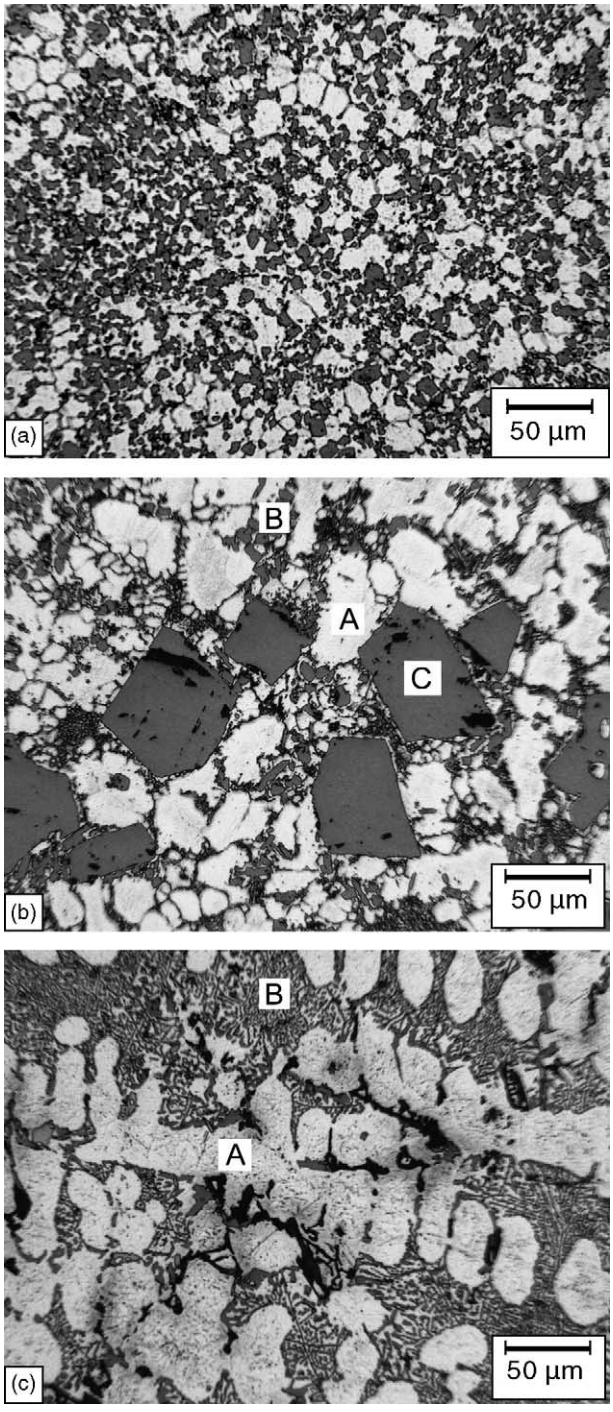

Fig. 2. Optical microstructures of the as prepared Al–Si–Cu–Mg alloys. (a) Al–25SiCuMg (PT); (b) Al–25SiCuMg (IT); and (c) LM13: (A) α-aluminum; (B) eutectic silicon particles; and (C) primary silicon particles.

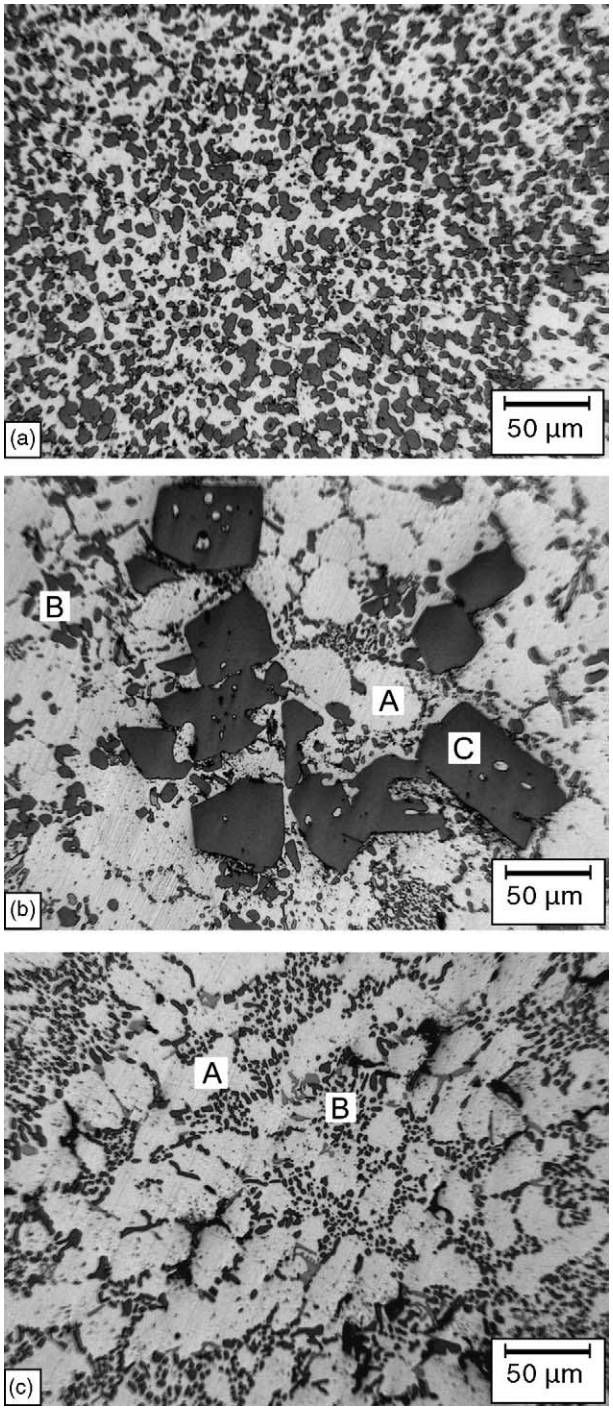

Fig. 3. Optical microstructures of the T6-treated Al–Si–Cu–Mg alloys. (a) Al–25SiCuMg (PT); (b) Al–25SiCuMg (IT); and (c) LM13 alloys: (A) α-aluminum; (B) eutectic silicon particles; and (C) primary silicon particles.

Table 2
Hardness values obtained on matrix of the alloys

Alloy	Heat treatment	Hardness (Hv, 100 gf)
Al–25SiCuMg (PT)	As thixocast	144
	T6	175
Al–25SiCuMg (IT)	As thixocast	108
	T6	152
LM13	As cast	86
	T6	141

however, the Al–25SiCuMg (IT) alloy contains coarse primary Si particles distributed unevenly in a matrix that comprises globular α-Al grains and polygonal eutectic Si particles (Fig. 2b). Finally, the LM13 alloy has the typical microstructure of an Al–12 wt% Si eutectic alloy that includes dendritic α-Al grains and fine needle-like eutectic Si particles (Fig. 2c). After T6 treatment, the primary Si particles in all the three alloys are more spherical and round, and the eutectic Si particles in Al–25SiCuMg (IT) and LM13 alloys are coarser (comparing Fig. 3 with Fig. 2).

Table 2 presents the microhardness values obtained on the matrix of the Al–Si–Cu–Mg alloys. T6 heat treatment improves the microhardness of all the alloys. The powder thixocast Al–25SiCuMg (PT) alloy has the highest microhardness and LM13 the lowest of all alloys in either as-prepared or T6 states.

3.2. Wear rate and coefficient of friction

Fig. 4 plots the wear rates (m^3/m) of the Al–Si–Cu–Mg alloys as a function of applied sliding load. Fig. 5 presents examples of the measured results of the coefficients of friction that were continuously recorded by measuring the frictional traction during sliding tests. A series of figures like that in Fig. 5 yields the mean coefficients of friction, which vary with the load for various alloys. Fig. 6 plots the variations in such coefficients.

The wear rates and coefficients of friction for the powder thixocast Al–25SiCuMg (PT) alloy were divided into three regions I–III (Figs. 4–6). In region I, the wear rate for the alloy increased almost linearly with the load; meanwhile, the coefficient of friction remained almost constant. The wear rate began to fall as the load increased to a critical value of about 67 N, a transition to region II; meanwhile, the coefficient of friction came to increase with the load in region II. This trend was followed by an increase in wear rates, which was accompanied by a decline in the coefficient of friction with the load in region III. Finally, the specimen underwent seizure. However, the two conventional alloys—Al–25SiCuMg (IT) and LM13—did not exhibit the similar wear regions II or III of the Al–25SiCuMg (PT) alloy at high load.

At low loads (region I), the three alloys in the as-prepared state have similar wear resistance (Fig. 4a), whereas Al–25SiCuMg (PT) in T6 state exhibited the much low

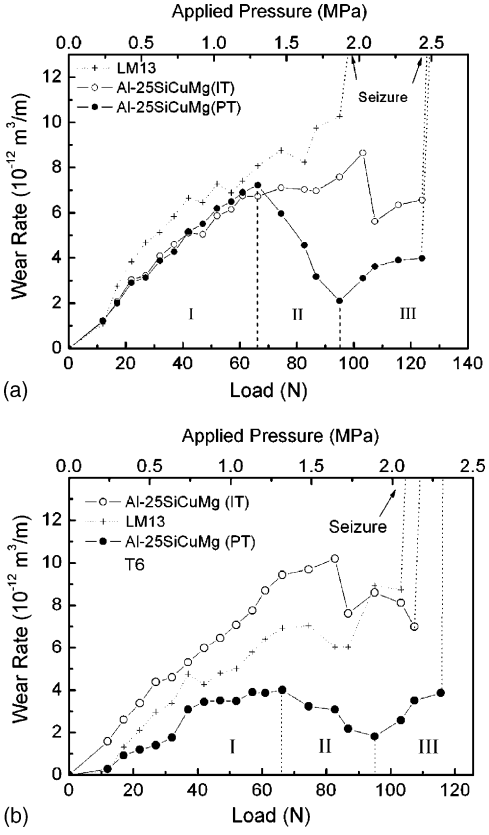

Fig. 4. Wear rates varied with load for the (a) as prepared and (b) T6-treated Al–Si–Cu–Mg alloys. The three regions denoted by I–III are shown for Al–25SiCuMg (PT) alloy.

wear rate than did the conventional alloys (Fig. 4b). At high loads (region II/III), Al–25SiCuMg (PT) alloys in both as-prepared and T6 state exhibited greater wear resistance than did the conventional alloys—Al–25SiCuMg (IT) and LM13 (Fig. 4).

Following T6 treatment, all the Al–Si–Cu–Mg alloys except Al–25SiCuMg (IT) showed improved wear resistance (comparing Fig. 4b with Fig. 4a). The effects of T6 treatment on the wear resistances of Al–25SiCuMg (PT) and Al–25SiCuMg (IT) alloys differed, although the two alloys were similarly composed. T6 treatment greatly increased the wear resistance of Al–25SiCuMg (PT) alloy, but reduced that of Al–25SiCuMg (IT) alloy, even though it increased the microhardness of Al–25SiCuMg (IT) alloy (Hv 152 against 108 in Table 2). Fig. 4 also reveals that Al–25SiCuMg (PT) had the highest seizure resistance in both as-cast and T6 state and LM13 alloy (∼12 wt% Si) had a lower seizure resistance than hypereutectic Al–25SiCuMg (PT) and (IT) alloys (>12 wt% Si).

Fig. 5 demonstrates that LM13 alloy exhibits similar wear behaviors to Al–25SiCuMg (PT), except in that that it does not have the behavior of region II. As the wear tests progressed, the coefficients of friction for both Al–25SiCuMg (PT) and LM13 alloys soon reached to a stable value of about 0.5 (region I in Fig. 5). As the applied load was further in-

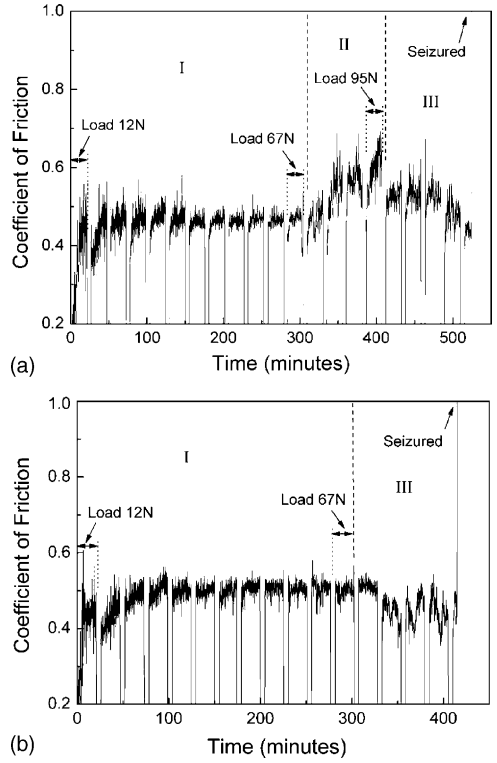

Fig. 5. Coefficients of friction as a function of sliding time for the as prepared (a) Al–25SiCuMg (PT) and (b) LM13 alloys.

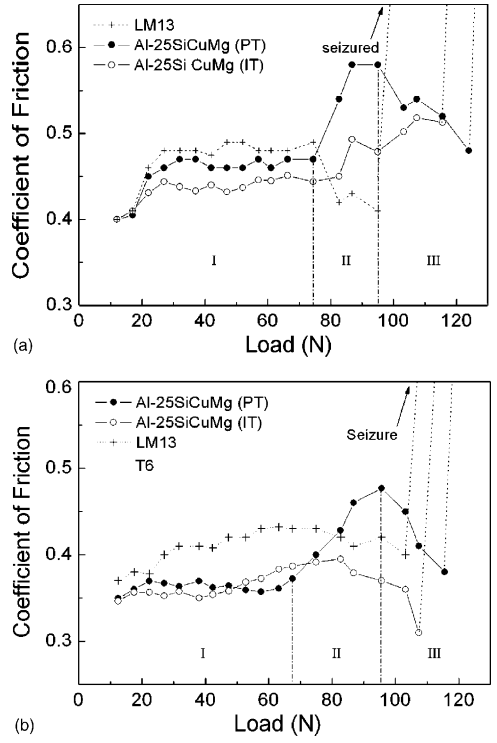

Fig. 6. Coefficients of friction as a function of load for (a) as prepared and (b) T6-treated Al–Si alloys.

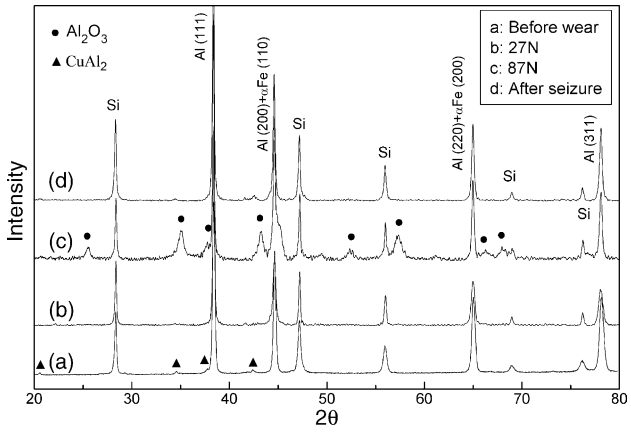

Fig. 7. XRD analyses obtained on the worn surfaces of the as prepared Al–25SiCuMg (PT) alloy (a) before wearing and (b) after wearing at a load of 27 N; (c) at a load of 87 N; and (d) after seizure occurring.

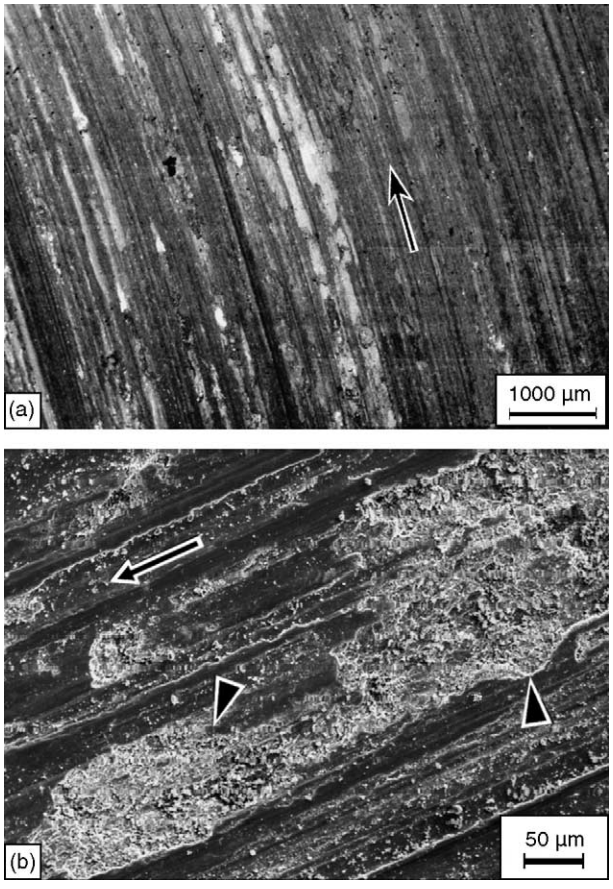

Fig. 8. (a) BEI micrograph of a worn surface tested at a load of 27 N for the Al–25SiCuMg (PT) alloy; white strips are verified to be Fe-rich areas. (b) SEI micrograph magnified from the worn surface shown in (a). Triangle arrows indicates the cavities across the sliding tracks, long arrows indicates the sliding direction (BEI: back-scattered electron image; SEI: secondary electron image).

creased to a critical value of around 67 N, the coefficient for Al–25SiCuMg (PT) increased (Fig. 5a); however, the coefficient of LM13 declined (Fig. 5b).

The coefficients of friction at low loads (region I in Fig. 6) substantially follow the order, LM13 > Al–25SiCuMg (PT) > Al–25SiCuMg (IT), for both the as-prepared and the T6-treated Al–Si alloys. All the coefficients of friction of the as-prepared and T6-treated Al–Si–Cu–Mg alloys exhibited a transition from stable to unstable states at a load of approximately 67 N (Fig. 6a and b). The T6-treated alloys exhibited lower coefficients of friction than the as-prepared alloys (comparing Fig. 6b with Fig. 6a).

3.3. Worn surfaces and debris

Fig. 7 presents the XRD spectra from the worn surface of the Al–25SiCuMg (PT) alloy after sliding under various loads. Before sliding, the surface was found to contain α-Al, Si and a little Al_2Cu (Fig. 7a). After it had been worn at 27 N, the surface had constituents similar to those before wearing (Fig. 7b). When the load increased to 87 N, the worn surface had a notable quantity of α-Al_2O_3 oxide (Fig. 7c), suggesting that a remarkable oxidation had occurred during sliding under such a high load. Fig. 7c did not reveal any Fe–Al or Fe–Al–O intermetallic phases on the worn surface, indicating that most of the iron that was transferred from disc surface may only be mechanically mixed with aluminum alloys or turned into nano-sized Fe–Al or Fe–Al–O compound particles. Finally, the oxide that had formed earlier on the worn surface disappeared after seizure (Fig. 7d), revealing that the oxide layer was removed during sliding under seizure load.

SEM observations indicated that all of the worn surfaces of the three Al–Si–Cu–Mg alloys had similar appearances when they were worn under similar loads. At low loads, worn surfaces of the alloys exhibited many parallel tracks or grooves, across which were numerous cavities (Fig. 8). As the load increased, the worn surfaces exhibited fewer cavities and greater plastic deformation. Fig. 9 presents the worn surface of Al–25SiCuMg (PT) alloy after it was worn at 87 N. On the worn surfaces, many white strips were observed in the direction of slip. EDS examination indicated that more iron and fewer oxygen were present in the white strip areas (Fig. 9c) than in the other, black areas (Fig. 9d). Fig. 10 shows a typical SEM micrograph perpendicular to the Al–25SiCuMg (PT) surface worn at 87 N. A mechanical mixing layer (MML) [19–21] was clearly found to cover the worn surface to a depth of 10 to 50 μm. The MML comprised iron and oxygen, as revealed by the EDS analysis shown in Fig. 10b.

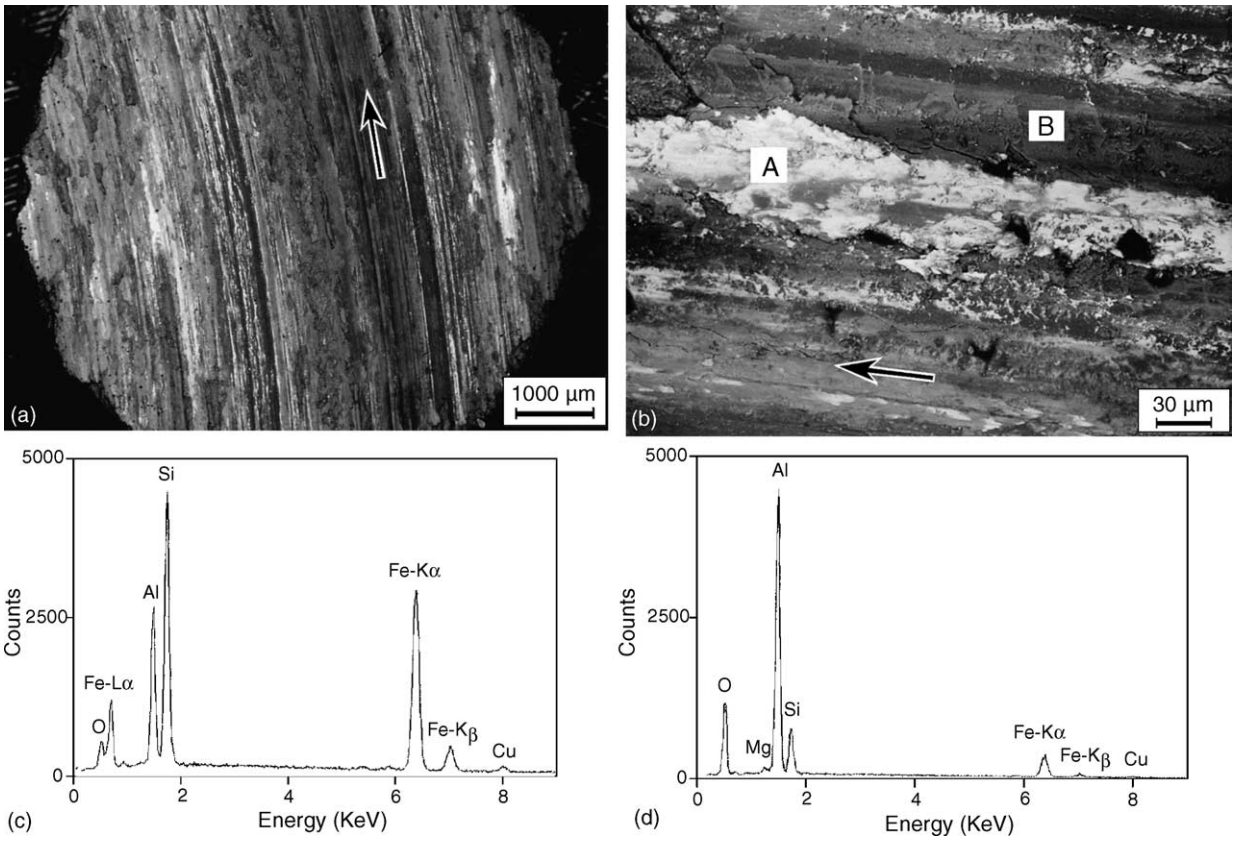

Fig. 9. (a) BEI micrograph of a worn surface obtained on the Al–25SiCuMg (PT) alloy tested at a load of 87 N; (b) BEI micrograph showing the magnified image of the worn surface; (c) and (d) are EDS spectra obtained from the area (A) and area (B), respectively (BEI: back-scattered electron image; EDS: energy dispersive spectrum).

Fig. 11 depicts the wear debris obtained from the sliding of Al–25SiCuMg (PT) at 87 N. The wear debris consists of three types of particles—plate-like flakes, equiaxed particles, and long flakes (Fig. 11a). The long flakes are believed to be the debris delaminated from the iron-rich strip whose area is shown in Fig. 9b, since these strip areas were also found to yield similar EDS spectra that is displayed in Fig. 9c. The size of the equiaxed particles ranges from submicron to several tens of microns (Fig. 11b). Indeed, all the Al–Si alloys tested herein were found to yield similar wear debris and the amount and size of the long iron-rich flakes and plate-like flakes increased with the sliding load.

Fig. 12 presents the typical cross-section optical micrographs of the subsurface for the worn Al–Si–Cu–Mg alloys after seizure. Fig. 12a demonstrates that Al–25SiCuMg (PT) had numerous small particles dispersed in the matrix near the worn surface. The dispersed particles were finer as they were nearer to the worn surface. The small dispersed particles contained the Si particles and the intermetallic compounds that were fragmented during sliding. A few small cracks are observed near the worn surface of the Al–25SiCuMg (PT) alloy (Fig. 12a). However, many large cracks initiated from the fracture of the primary Si particles were found near the worn surface of the Al–25SiCuMg (IT) alloy (Fig. 12b). The α-Al grains in Fig. 12b were elongated in the direction of sliding, suggesting extensive plastic deformation under the surface of Al–25SiCuMg (IT). LM13 alloy also underwent an extensive deformation near the worn surface (Fig. 12c). The maximum depth of deformation below the worn surface in the present cross-sectional micrographs is about 100 μm.

Fig. 13a and b show the optical microstructures of subsurfaces worn at 12 N and 87 N, respectively. The subsurface worn at 12 N showed no plastic deformation; several primary Si particles were found to protrude from the worn surfaces (Fig. 13a), suggesting that the primary Si particles may act as asperities and carry the load during sliding. The MMLs formed on the surface at high load were found to include various fragmented Si particles (Fig. 13b).

3.4. Sliding surface temperature

The surface temperatures were measured using a thermal couple in contact with the worn surface after sliding for 20 min. These measured temperatures are regarded as the bulk surface temperatures in the steady state. Fig. 14 presents the measured surface temperature of the as-prepared Al–Si–Cu–Mg alloys. T6-treated alloys exhibited similar trends in temperature, but the values were slightly smaller than those of the as-prepared alloys. At low loads, below about 70 N, LM13 alloy was found to have the highest measured temperature, and Al–25SiCuMg (IT) alloy to have the lowest measured temperature. However, as the load further increased, the temperature of Al–25SiCuMg (PT) alloy slowly came to exceed that of the other two alloys (Fig. 14).

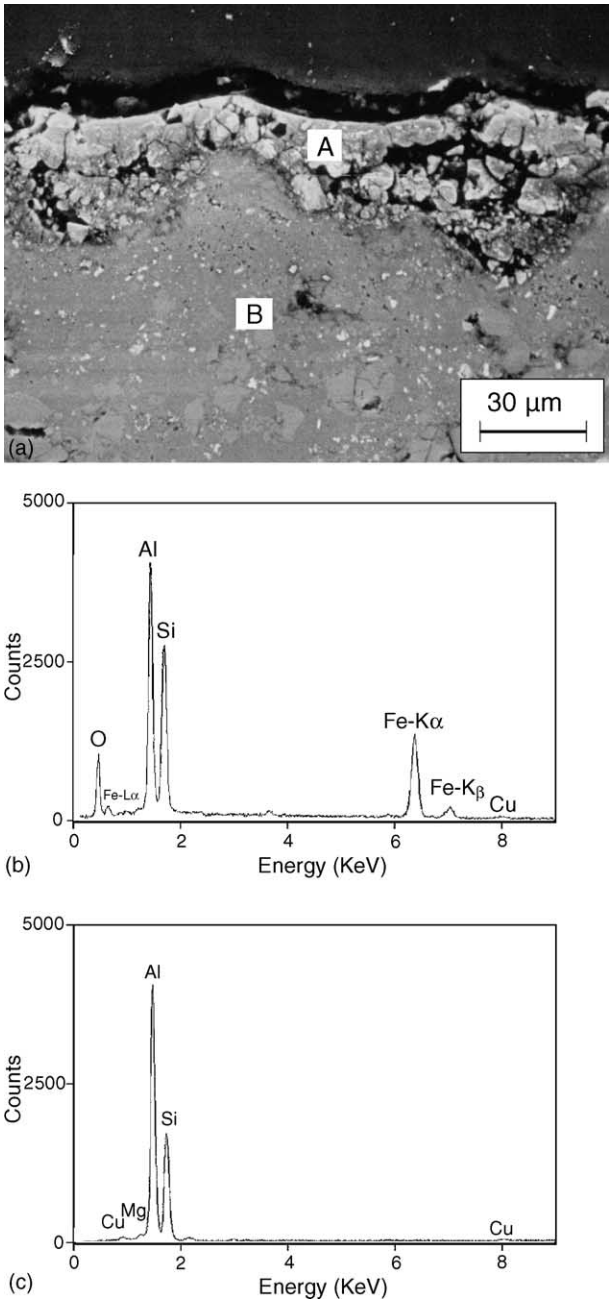

Fig. 10. (a) BEI micrograph of a cross-section perpendicular to the worn surfaces for the Al–25SiCuMg (PT) alloy tested at 87 N. The sliding direction is perpendicular to the paper; (b) and (c) are EDS spectra obtained from the area (A) and area (B), respectively (BEI: back-scattered electron image; EDS: energy dispersive spectrum).

4. Discussion

The wear rate of an Al–Si/steel sliding system normally involves mild and severe wear regions, according to the applied load [22]. At low load, the wear rate increases almost linearly with the load, as in mild wear; at high loads, the wear rate increases very rapidly with load, as in severe wear [22]. The mild wear can be the wear of region I (Fig. 4); whereas, the severe wear may correspond to the wear of region III herein

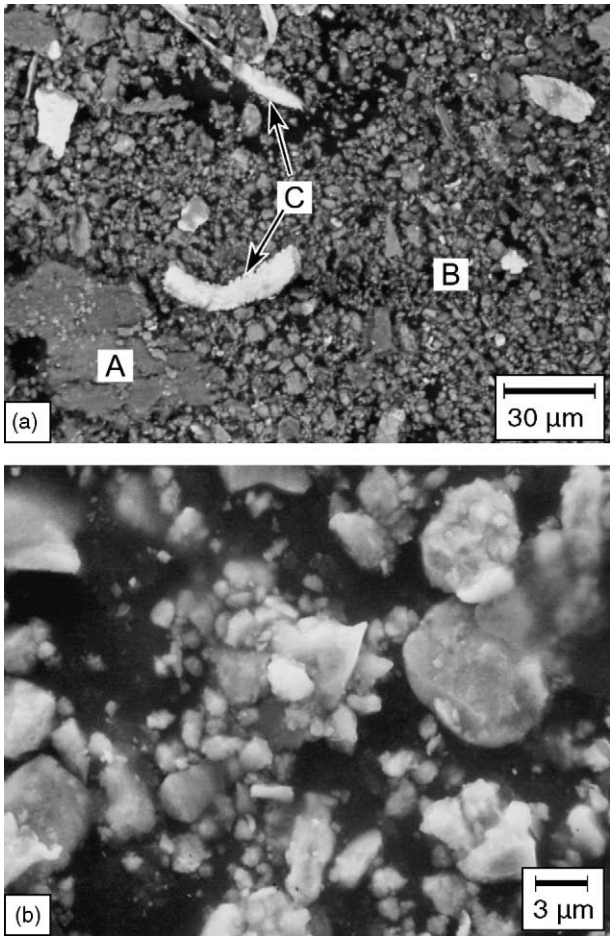

Fig. 11. The wear debris obtained in the Al–25SiCuMg (PT)/steel wearing system at a load of 87 N. (a) A typical BEI micrograph, showing a mixture of (A) plate-like flakes; (B) fine equiaxed particles; and (C) long iron-rich flakes. (b) A magnified secondary electrons image (SEI) of the fine equiaxed particles.

(Fig. 4). However, region II (Fig. 4) observed for the powder thixocast alloy in this study involved a drop in wear rate with load. The drop in wear rate with load is rather unusual and differs from the mild and severe wear. In fact, the region II has seldom been reported for conventional Al–Si alloys [22]. The wear results and mechanisms of the three wear regions I–III are discussed as follows.

4.1. Wear behaviors at low loads (region I)

4.1.1. Wear rate—the influence of matrix hardness and size of Si particles

The wear rates of the Al–Si–Cu–Mg alloys at low loads increased linearly with the load (Fig. 4). The linearity can be explained using the Archard model [23]. When wear is tested at low loads, plastic deformation is localized at the real contact spots or asperities on the sliding surfaces. In the Archard model, the wear loss is hypothesized to be related to the volume of the debris detached from the real contact asperities that have been plastically deformed and adhere to a counter

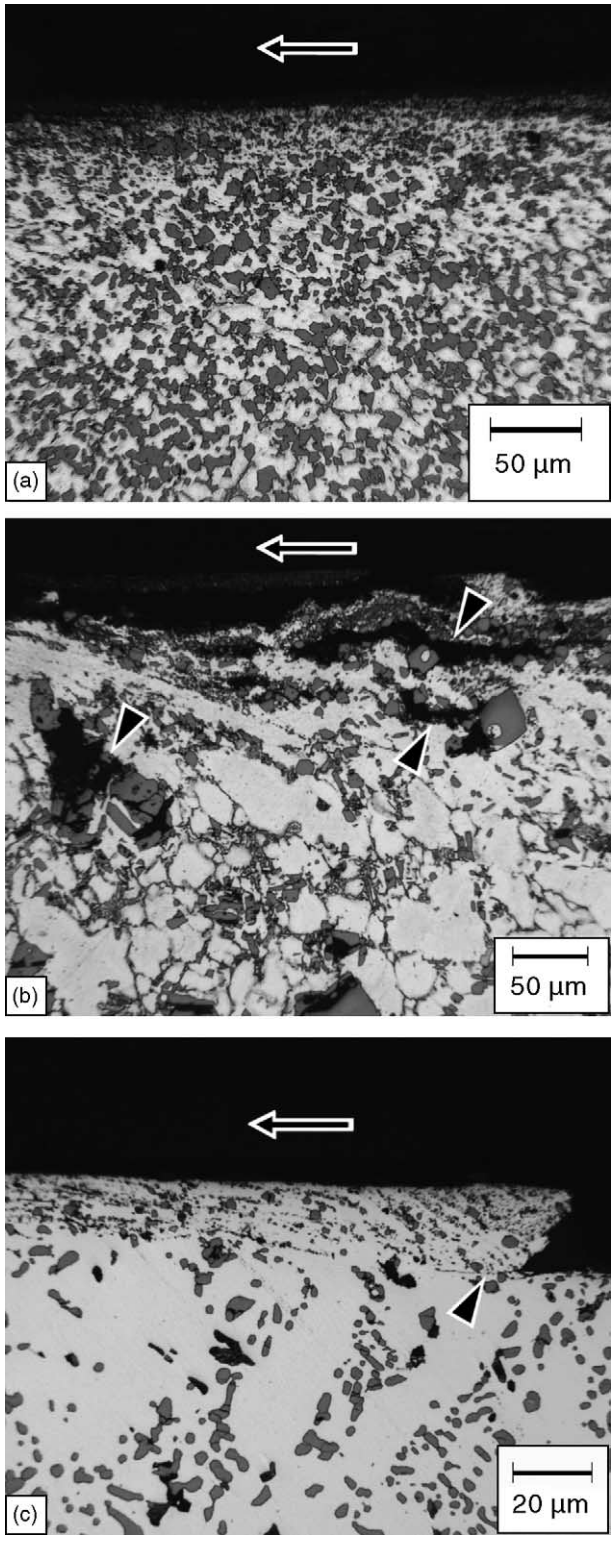

Fig. 12. Optical micrographs of cross-sections perpendicular to the worn surfaces after seizure and parallel to the sliding direction for (a) as prepared Al–25SiCuMg (PT); (b) as prepared Al–25SiCuMg (IT); and (c) T6-treated LM13 alloys. Plastic deformation were found in the subsurface with depth of 20–100 μm. The upper arrows indicate the sliding direction, and the triangle arrows indicate the cracks in the subsurfaces.

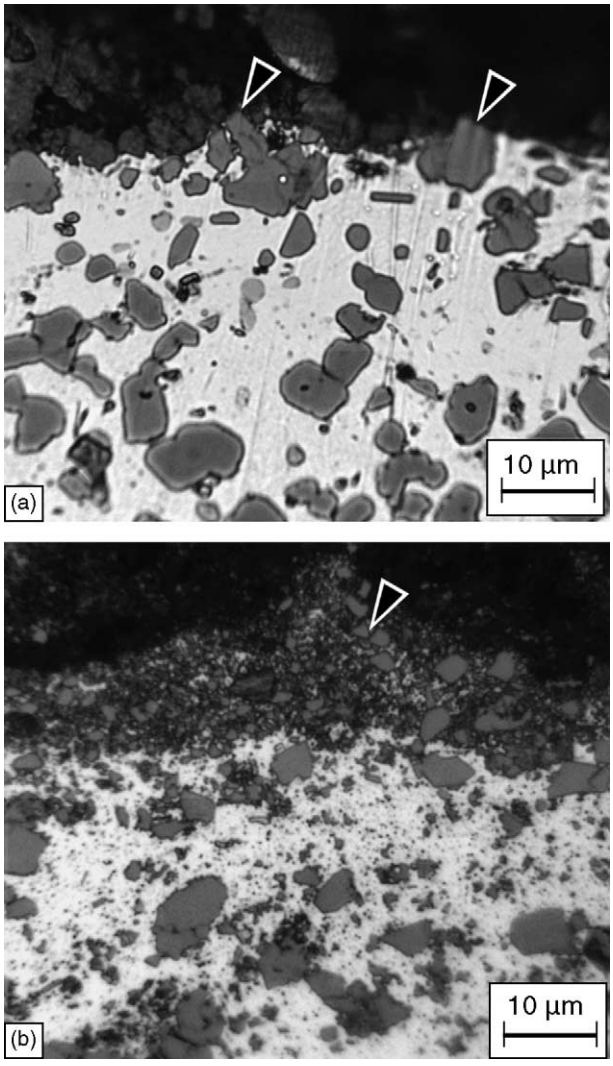

Fig. 13. Optical microstructure of the subsurfaces obtained from as prepared Al–25SiCuMg (PT) alloy after sliding at (a) 12 N and (b) 87 N. The sliding direction is perpendicular to the paper. Arrows indicate the asperities protruding from the sliding surfaces.

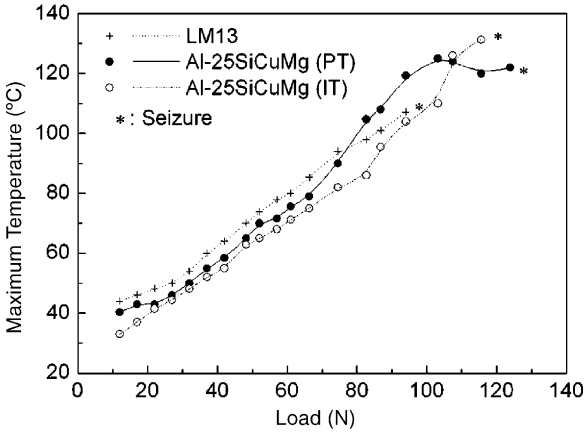

Fig. 14. Variation with load of sliding surface temperature for the as prepared Al–Si–Cu–Mg alloys.

surface. Based on this assumption, the volume of wear (W) after sliding through a distance (d) is given by $W/d=(KL)/(3H)$, where K is a wear rate constant; L is the nominal applied force, and H is the penetration hardness of the surface material that is being worn away.

Harder materials are expected to have greater wear resistance, according to the Archard model. The Al–25SiCuMg (PT) alloy in T6 condition has the highest hardness of all the tested alloys (Table 2). This fact explains why the T6-treated Al–25SiCuMg (PT) alloy had a much lower wear rate than the others at low loads (Fig. 4b). However, this study found an exception of the relationship between the wear rate and the hardness in the Archard model. Al–25SiCuMg (IT) alloy had a lower wear resistance than LM13 in T6 condition (Fig. 4b), although the hardness exceeded that of the latter (152 Hv against 141 Hv). This exception is associated with the large primary Si particles in Al–25SiCuMg (IT) (Fig. 3b). The large Si particles tend to be fractured (Fig. 12b) and worn off during sliding, increasing the wear rate of the alloy. This problem of the effect of large primary Si particles on the wear performance of hypereutectic alloys has been discussed [15]. Accordingly, the superior performance of the T6-treated Al–25SiCuMg (PT) follows from not only the high microhardness of the alloy but also the unique characteristics of fine and uniform Si particulates fabricated by powder thixocasting process in this work.

4.1.2. Coefficients of friction—the influence of morphology of Si particles

The size and distribution of the primary Si particles in the Al–Si alloys are suggested to affect greatly the coefficients of friction. Fig. 15 schematically depicts the cross-sections of the three Al–Si–Cu–Mg alloys during sliding, to elucidate the mechanisms for the frictional traction. These diagrams were based on the microstructural observations of the worn subsurfaces. The model in Fig. 15 may explain why the coefficients of friction follow the order, LM13 > Al–25SiCuMg (PT) > Al–25SiCuMg (IT), under the same wearing conditions, at low loads (region I in Fig. 6).

In Fig. 16, the materials just below the worn surface showed no plastic deformation at low loads. As sliding proceeded, some of the primary Si particles protruded from the worn surfaces (Fig. 13a). During the initial stage of sliding, the hard Si protuberances may plough the steel counter surface, causing material to be transferred from the steel surface, so separated thin iron-rich strips were formed on the aluminum worn surfaces (Fig. 8a).

The actual contacts between the sliding surfaces are well known to be localized only at some individual spots, called asperities, on a microscopic scale. The higher affinity of the asperities to adhere to the steel counter surfaces results in the larger frictional traction during sliding. Fig. 15 depicts the primary Si particles protrude from the worn surfaces during slide wearing. These protrusions may act as points of contact with the steel counter body to carry most of the sliding load. The larger Si particles are responsible for the

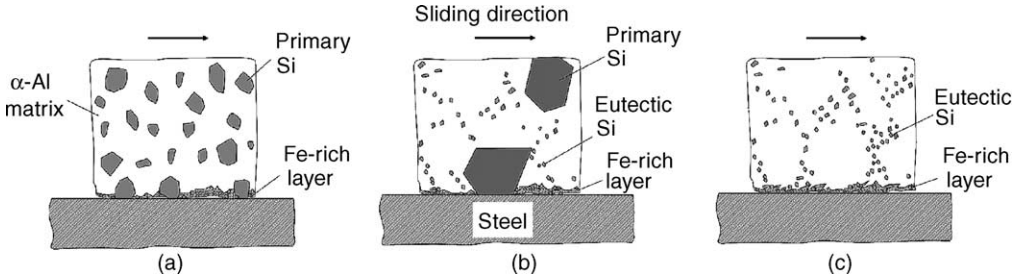

Fig. 15. Schematic diagrams of the cross sections perpendicular to the sliding surfaces at low loads: (a) Al–25SiCuMg (PT); (b) Al–25SiCuMg (IT); and (c) LM13 alloys.

generation of the larger protuberances on the worn surfaces, reducing the opportunity for the α-Al matrix to come into contact with the steel counterbody, reducing the frictional traction.

Greater contact of aluminum asperities is responsible for higher frictional traction because aluminum is prone to adhere to a steel surface. However, stronger contact of Si particles corresponds to lower frictional traction, because Si particles cannot easily adhere to the steel counterface and they may become fractured and thus acts as a solid lubricant. Hence, the larger primary Si particle or a higher Si content is postulated to reduce the frictional traction. This assertion is consistent with the fact that the LM13 (∼12% Si) alloy has a higher frictional traction at low load than the Al–25SiCuMg alloys (∼25% Si) and the coefficient of frictional for Al–25SiCuMg (IT) alloy is lower than that for Al–25SiCuMg (PT) alloy in region I of Fig. 6.

4.2. Wear behaviors at high loads (region II/III)

4.2.1. Mechanical mixing layer (MML) formed on sliding surfaces

Fig. 16 depicts a schematic diagram to elucidate the wear behaviors of the Al–25SiCuMg (PT) alloy at high load. This proposed figure is based on the microstructural observations of the worn surfaces and subsurfaces.

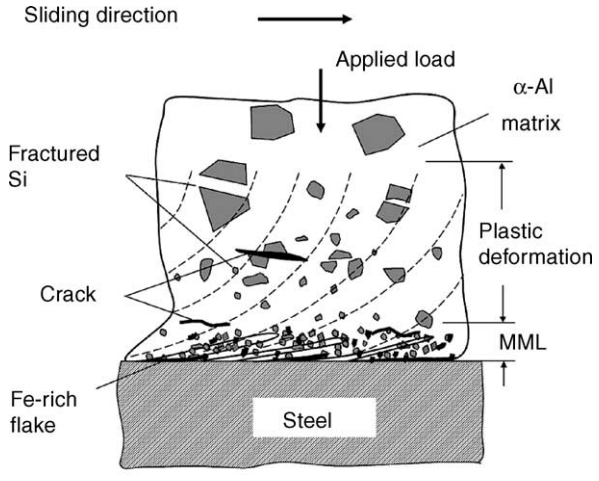

Fig. 16. Schematic diagrams of the cross section perpendicular to the surface sliding under heavy load for the hypereutectic Al–Si alloys.

In Fig. 16, a plastic deformation zone below the worn surface is exhibited. In this deformation zone, many cracks are initiated from the sites of the fractured Si particles, suggesting that large flakes of debris may be detached from these cracks. A mechanical mixing layer is present on the worn surface of the alloy. Some cracks are present in the MML, which is deduced from the fact that long Fe-rich flakes were present in the debris (Fig. 11a) and these flakes are posited to be delaminated from the cracks in the MMLs.

The MML commonly forms on the sliding surface of an Al–Si alloy when it slides against a steel counter body [19–21]. It is generated by the mutual transfer of materials between the two contact surfaces and is normally accompanied by an extensive surface deformation. The compositions and microstructures in the MML also vary with the sliding load. At low load, the MML consists of a matrix of ultrafine α-Al grains dispersed with small α-Fe particles, and no intermetallic compound or oxides are generated at low load; whereas, at high loads, the MML consists of nanosized particles of Fe–Al(Si) intermetallic compounds, aluminum and iron oxides that are dispersed in the ultrafine α-Al matrix [20,21]. The MML contains these ultra-fine microstructures, and so can effectively protect the surface from wear.

These microstructural characteristics of the MML described in [20,21] match those identified herein. At low loads, several Fe-rich strips were present on the sliding surfaces (Fig. 8a). These Fe-rich strips can be regarded as a species of MML that is formed at low load. However, the Fe-rich strips formed at low loads should be very thin, since there was little subsurface deformation occurred as depicted in Fig. 16. As the sliding load was increased, a significant quantity of aluminum oxide was detected on the worn surface (Fig. 7c). The formation of oxide is consistent with that in [20], which states that the sliding surface of Al–Si alloys may be oxidized by the oxidizing atmosphere and the increase in the high surface temperature by the heavy sliding load. The MML formed at high load was found to include Fe element (Fig. 10b), and many fine Si particles embedded in a severely deformed Al matrix (Fig. 13b). The MML formed at high load was also determined herein to exhibit very high hardness, of up to approximately 600 Hv.

4.2.2. Transition of wear region I to II – the influence of subsurface deformation

A transition of the wear rate from region I to region II is evident for the powder thixocast Al–25SiCuMg (PT) alloy in both as-prepared and T6 states (Fig. 4). The transition is important for the powder thixocast alloy because it clearly dramatically improve the wear performance of this alloy under high-load sliding conditions.

Section 4.2.1 describes that the formation of MMLs can effectively protect the surfaces from wear. However, the wear rate of Al–25SiCuMg (PT) continuously increased with the load below 67 N (region I in Fig. 4), in spite of the production of the MMLs. In contrast, the wear rate began to drop as the load increased to 67 N (Fig. 4). The MMLs were generated under a wide range of loads for Al–Si/steel sliding systems [24–26], but the transition is related only to a critical load. This difference reveals that the MMLs formed at high loads (in region II) seem to be much "stronger" than those formed at low loads (in region I).

The fact that the "stronger" MMLs are formed at high loads is attributable to the plastic deformation and the oxidation on the surface or subsurface material. Two factors can mainly affect the strength of the Al–Si surface during sliding wear—the rise in surface temperature and the intention of subsurface plastic deformation. A high surface temperature usually softens the sliding surface material by dynamic recovery or recrystallization or coarsening of age-hardened precipitates [26]. However, plastic deformation strengthens the surface material by work hardening, generating microstructures that comprise elongated subgrains or textures [24–26]. Additionally, a large plastic deformation may also involve ultra fine oxides or intermetallic compound particles dispersed in the subsurface matrix through a process that is similar to mechanical alloying [24]. Consequently, the transition observed herein is suggested to be "triggered" by a critically intense subsurface deformation, as it was accompanied by the "stronger" MMLs.

The coefficient of friction on the Al–25SiCuMg (PT) alloy became rising and unstable when the load increased to the transition point, 67 N (Fig. 5a). This rising in the coefficient of friction at the transition can be explained using the aforementioned suggestion that an extensive subsurface deformation should be responsible for the transition. In beginning of the wearing test, the large Si particles that protrude from the surfaces served as points of contact during sliding at low loads (Fig. 15). These protruding Si particles prevented the α-aluminum matrix from touching and adhering to the steel counter surfaces. Accordingly, the Al–25SiCuMg (PT) alloy had a low coefficient of friction at low load (region I in Fig. 5a), since the Si particles have a low affinity to the counter surface. However, as the sliding proceeded, the temperature of the sliding surface increased continuously with the sliding load (Fig. 14), gradually softening the α-aluminum matrix. When the external stress yielded by the frictional traction and the applied load exceeded the flow strength of the aluminum matrix, the aluminum matrix would begin to be plastically deformed. Consequently, the plastic flow of the matrix fractured the primary Si particles (Fig. 16). As the large primary Si particles were broken down into small particles, the aluminum matrix came into contact with, and adhered to, the steel counter surface, increasing the coefficient of friction (region II in Fig. 5a) because of the high affinity of aluminum to the steel surface.

However, the coefficient of friction of LM13 was found to drop as the load increased to the transition load of above 67 N (Fig. 5b). The behavior of the LM13 alloy is exactly opposite that of the Al–25SiCuMg (PT) alloy (Fig. 5a and b). This drop in the coefficient of friction is regarded as similar to the behavior of region III for the powder thixocast alloy presented in Fig. 5a, because the as-prepared LM13 alloy did not give any drop in wear rate at high loads, as displayed by the powder thixocast alloy in the region II (Fig. 4a). The drop in the coefficient of friction in region III for the Al–Si alloys is attributable to the softening of the material at its sliding surface and the high wear rate during sliding at high loads. Table 2 shows that LM13 has lower microhardness than Al–25SiCuMg (PT) alloy, revealing that LM13 alloy could have more intense plastic deformation than that did Al–25SiCuMg (PT) alloy during heavy load sliding. However, the large deformation of LM13 at high loads also accelerates the formation of wear debris by delamination [27]. Moreover, the large amount of wear debris may act as a solid lubricant, reducing the ability of the "fresh" aluminum matrix to adhere to the steel counterbody and thereby reducing the frictional traction in region III (Fig. 5b). In contrast, the Al–25SiCuMg (PT) alloy was found to have a very low wear rate in region II (Fig. 4), suggesting that the protective MMLs formed on the sliding surface were more stable for Al–25SiCuMg (PT) than for LM13. Hence, the reduction by the debris lubricant of the coefficient of friction for the Al–25SiCuMg (PT) alloy is weak, leading to the different behaviors in the coefficient of friction between Al–25SiCuMg (PT) and LM13 when the sliding load was increased just above 67 N (Fig. 5a and b).

From the above discussions, it is therefore concluded that the superior wear performance for Al–25SiCuMg (PT) alloy is not only because of its high hardness but also because of its fine primary Si particles through the unique process of powder thixocast, since the fine Si particles can effectively suppress the delaminating rate of MMLs.

5. Conclusions

Dry sliding wear behaviors of a powder thixocast alloy—Al–25Si–2.5Cu–1Mg (PT)—were investigated. For comparison, the wear performances of two alloys—Al–25Si–2.5Cu–1Mg (IT) and LM13, fabricated by conventional casting routes were also examined. The following conclusions are drawn.

1. The powder thixocast Al–25Si–2.5Cu–1Mg (PT) alloy shows greater resistance to wear, finer and more uniform microstructures than the conventional alloys.

2. The plots of the wear rate of the powder thixocast alloy varied with the load and could be divided into three regions. The wear rate increased about linearly with the load below 67 N (region I); it then slowly decreased as the load increased from 67 N to 97 N (region II). It finally slowly increased to seizure (region III). The transition from wear region I to region II is attributable to the formation of the mechanical mixed layer generated by plastic deformation of a heavy loaded worn surface. The transition from wear region II to region III is probably governed by the delamination of MML under more severe load conditions.
3. The MMLs formed at high loads herein contain plenty of Si, Fe, and Al_2O_3 phases embedded in an α-Al matrix. The formation of the MMLs was accompanied by a large plastic deformation of the material that is adjacent to the sliding surface.
4. The formation of stable mechanical mixing layers on sliding surfaces is responsible for the superior wear performance of the powder thixocast alloy. In contrast, the formation of MMLs was found to have less beneficial effect on the conventional Al–Si–Cu–Mg alloys. This difference is attributable to the fact that the delamination rate of MMLs in the conventional alloys is higher than that in the powder thixocast alloy because subsurface cracks tend to be generated from the sites of the fractured large Si particles or the soft matrix of the conventional eutectic Al–Si–Cu–Mg alloys.

Acknowledgements

The authors would like to thank the National Science Council of the Republic of China for financially supporting this research under Contract No. NSC 91-2216-E-009-022.

References

[1] J.E. Hatch, Aluminum: Properties and Physical Metallurgy, ASM, Ohio, 1984.
[2] J.E. Gruzleski, B.M. Closset, The Treatment of Liquid Aluminum–Silicon Alloys, AFS, Illinos, 1990.
[3] Kiyoaki Akechi, US Patent 4:838,936 (1989).
[4] H. So, W.C. Li, H.K. Hsieh, J. Mater. Process. Technol. 114 (2001) 18–21.
[5] C.M. Chen, C.C. Yang, C.G. Chao, Mater. Sci. Eng., A 366 (2004) 183–194.
[6] C.M. Chen, C.C. Yang, C.G. Chao, Int. J. Cast Met. Res. 17 (2004) 174–181.
[7] M.C. Flemings, Metall. Trans. A 22 (1991) 957–981.
[8] A.D. Sarkar, Wear 31 (1975) 331–343.
[9] J. Clarke, A.D. Sarkar, Wear 54 (1979) 7–16.
[10] F. Wang, H. Liu, Y. Ma, Y. Jin, Mater. Des. 25 (2004) 163–166.
[11] S.C. Lim, M. Gupta, Y.F. Leng, E.J. Lavernia, J. Mater. Process. Technol. 63 (1997) 865–870.
[12] L. Lasa, J.M. Rodriguez-Ibabe, Scr. Mater. 46 (2002) 477–481.
[13] L. Lasa, J.M. Rodriguez-Ibabe, Mater. Sci. Eng., A 363 (2003) 193–202.
[14] F. Wang, Y. Ma, Z. Zhang, X. Cui, Y. Jin, Wear 256 (2004) 342–345.
[15] B.K. Prasad, K. Venkatesearlu, O.P. Modi, A.K. Jha, S. Das, R. Dasgupta, A.H. Yegneswaran, J. Mater. Sci. Lett. 17 (1998) 1381–1383.
[16] C. Subramanian, Wear 151 (1991) 97–110.
[17] B.K. Yen, T. Ishihara, Wear 198 (1996) 169–175.
[18] M. Acilar, F. Gul, Mater. Des. 25 (2004) 209–217.
[19] C. Subramanian, Wear 161 (1993) 53–60.
[20] X.Y. Li, K.N. Tandon, Wear 225-229 (1999) 640–648.
[21] X.Y. Li, K.N. Tandon, Wear 245 (2000) 148–161.
[22] A. Somi Reddy, B.N. Pramila Bai, K.S.S. Murthy, S.K. Biswas, Wear 171 (1994) 115–127.
[23] J.F. Archard, J. Appl. Phys. 24 (1953) 981–988.
[24] C. Perrin, W.M. Rainforth, Wear 203-204 (1997) 171–179.
[25] B.N. Pramila Bai, S.K. Biswas, J. Mater. Sci. 19 (1984) 3588–3592.
[26] X.Y. Li, K.N. Tandon, Wear 203-204 (1997) 703–708.
[27] N.P. Suh, Wear 25 (1973) 111–124.